Mössbauer Studies on ^{57}Fe Atoms in Rare-Gas Matrices between 1.45 and 20.5 K[†]

T. K. McNab,[*] H. Micklitz,[‡] and P. H. Barrett

Department of Physics, University of California, Santa Barbara,
Santa Barbara, California 93106
(Received 2 June 1971)

The Mössbauer absorption spectra of ^{57}Fe have been measured in the rare-gas matrices argon, krypton, and xenon with iron atomic concentrations from 0.3 to 3% and matrix temperatures between 1.45 and 20.5 K. All of the spectra show an absorption line with an isomer shift of $\delta = -0.75 \pm 0.03$ mm/sec with respect to an iron foil at 300 K. This isomer shift is independent of rare-gas matrix, iron concentration, and matrix temperature. This line is ascribed to an isolated ^{57}Fe atom (monomer) with an atomic configuration of $3d^6 4s^2$. The measured isomer shift gives a new calibration point in the isomer-shift–versus–electron-density plot for ^{57}Fe. The observed $1/T$ temperature dependence of the monomer linewidth shows that the direct phonon process is dominant in the spin-lattice relaxation mechanism. Spin-lattice relaxation times of the order of 2.5×10^{-10} sec are obtained by assuming a hyperfine field of 1.1×10^6 Oe at the ^{57}Fe nucleus due to an iron atom with unquenched orbital momentum. From the temperature dependence of the Mössbauer f factor, the Mössbauer temperatures Θ_M in the Debye model are calculated and compared with the values expected from specific-heat measurements. The Mössbauer spectra show, in addition to the monomer absorption line, a pair of narrow lines ($\Gamma = 0.22$–0.3 mm/sec), which is intensified with increasing iron concentrations. These lines can be interpreted as the result of the quadrupole splitting of the $I = \frac{3}{2}$ excited state of ^{57}Fe in the axial field produced by an iron nearest neighbor (dimer). The measured quadrupole splitting is $\Delta E_Q = 4.05 \pm 0.04$ mm/sec, and the isomer shift for the dimer is $\delta = -0.14 \pm 0.02$ mm/sec, corresponding to an effective atomic configuration of $3d^6 4s^x$ with $x = 1.47 \pm 0.04$. For ^{57}Fe in krypton and xenon, the measured dimer/monomer ratio is that which one would expect from probability considerations, but in argon it is a factor of approximately 3 higher than expected.

I. INTRODUCTION

Rare-gas–matrix-isolated atoms in neutral and charged states have been studied in the last twenty years by optical-absorption[1] and emission[2-4] spectroscopy and electron paramagnetic resonance.[5,6] These experiments indicate that the atoms trapped in the rare-gas matrix have properties very similar to those of the free atoms, demonstrating that the weak binding in these solids does not change the atomic configurations. In 1961 Jaccarino and Wertheim[7] proposed a Mössbauer experiment with rare-gas–matrix-isolated ^{57}Fe atoms to solve the problem of iron isomer-shift calibration. According to the results of optical spectroscopy, the Mössbauer isomer shift of a matrix-isolated ^{57}Fe atom would be approximately that of the free ^{57}Fe atom with the atomic configuration $3d^6 4s^2$. Re-

cently, several investigators have used the Mössbauer-effect technique to study the hyperfine interactions of ^{83}Kr in solid krypton[8-10]; however, these are not rare-gas–matrix-isolation experiments, since an impurity atom is not being studied. The first successful rare-gas–matrix-isolation Mössbauer experiment was carried out with iodine molecules (I_2) imbedded in a solid argon matrix at 22 K.[11] The results obtained in this experiment indicated that the isolated molecule indeed can be considered as an almost free entity where matrix interactions are negligible. The first results of a Mössbauer experiment with ^{57}Fe in an argon matrix at 4.2 K have been reported by Barrett and McNab.[12] Keune[13] attempted to isolate ^{57}Fe atoms in a neon matrix; however, his results indicated the presence of Fe_2O_3 and FeO clusters in the matrix. These Mössbauer spectra of ^{57}Fe in

4   3787

argon[12] showed, in addition to the single absorption line of isolated ^{57}Fe atoms, a pair of lines which was interpreted as a quadrupole splitting due to the interaction of iron pairs (^{57}Fe atoms, which have as one of their nearest neighbors another iron atom).

This paper reports experiments in which the Mössbauer effect of ^{57}Fe is observed in rare-gas matrices of argon, krypton, and xenon in the temperature region 1.45–20.5 K. The observation of the Mössbauer effect at different matrix temperatures and in different matrices gives, in addition to isomer-shift and quadrupole-splitting data, information about matrix annealing effects and about the interaction of rare-gas lattice vibrations with the ^{57}Fe atom, i.e., the mean-square displacement $\langle x^2(T)\rangle$ and the spin-lattice relaxation time of the ^{57}Fe atom.

II. EXPERIMENTAL APPARATUS AND OPERATING PROCEDURES

A detailed description of the apparatus and operating procedures for the iron matrix isolation has already been described elsewhere.[12,14] Only the main features of the experimental arrangement and of the matrix-isolation technique are explained here.

The samples are made in a liquid-helium cryostat, evacuated to a pressure of about 8×10^{-8} Torr (measured with liquid helium in the cryostat). A stream of rare gas enters the cryostat through an adjustable needle valve. It is mixed with an iron beam (70–90% enriched in ^{57}Fe), coming out of an alumina crucible contained in a resistance-heated tantalum furnace. The furnace temperature is held constant to within $\pm 5\,^{\circ}$C and is measured by a calibrated solar cell. Typically the flow rate was about 0.5 (cc STP)/min and the furnace temperature about 1270 °C. These conditions give a rare-gas/iron atomic ratio of about 100. The mixed rare-gas–iron beam condenses on a cooled beryllium disk, which is thermally bonded to the bottom of the liquid-helium or liquid-hydrogen bath. By pumping on this coolant bath, the temperature of the beryllium disk can be varied from 1.30 to 4.2 K or from 14 to 20.5 K. In this way, a change of the matrix temperature is possible. The estimated temperature gradient in a rare-gas layer of 5 mg/cm^2 is about 10 °C with a furnace temperature of 1300 °C and about 0.3 °C with an unheated furnace. The rare-gas deposition rate is continuously monitored by the attenuation of the iron 6.4-keV K x ray from a ^{57}Co-in-Cu source. The iron deposition rate is calculated through the experimentally determined collection efficiency of the beryllium disk by weighing the crucible before and after a run. The rare-gas/iron atomic ratio can thus be calculated within an error of

about $\pm 15\%$. The Mössbauer spectra were obtained with a conventional constant-acceleration spectrometer using a ^{57}Co-in-Pd source at 300 K, a krypton-filled proportional counter for detecting the 14.4-keV γ rays, and an enriched ^{57}Fe foil for calibration purposes.

III. EXPERIMENTAL RESULTS AND DISCUSSION
A. General Features

The Mössbauer spectra for ^{57}Fe in argon and krypton show the following features independent of the iron atomic concentration ϕ in the rare-gas matrix for $\phi \leq 0.03$ and the matrix temperature (over the range 1.45 K $\leq T \leq$ 20.5 K): a single broad central line, which narrows at higher temperatures, and two narrow lines on either side of the central line. Figure 1 shows as an example the spectra of ^{57}Fe in an argon matrix (Ar/Fe = 105 or $\phi \sim 0.01$) in which the matrix is cooled down from 17.5 to 1.45 K. The spectrum of ^{57}Fe in argon at 20.5 K was done after all the other temperature runs, because at this temperature there occurs migration and subsequently clustering of the iron atoms[1] (this is the interpretation of the absorption peak appearing between $v = 0.0$ and 1.0 mm/sec in the 20.5-K run). The intensity of the two narrow lines is greater in an argon matrix than in a krypton matrix (for the same iron concentration) and increases in both matrices with increasing iron concentration (see Fig. 2 as an example). The ^{57}Fe/Xe spectra show at all iron concentrations up to $\phi = 0.03$ and at temperatures between 4.4 and 27 K only the single central line (see Fig. 3, lower spectrum). Two small lines seem to be present in the 1.45-K-^{57}Fe/Xe spectrum at the position of the two narrow lines in argon and krypton (see arrows in Fig. 3, upper spectrum). The two narrow lines have a linewidth of $\Gamma = 0.22 \pm 0.2$ mm/sec for ^{57}Fe in the argon matrices, they seem to be broader for ^{57}Fe in krypton ($\Gamma = 0.30 \pm .05$ mm/sec), and the two weak lines appearing in the xenon run at 1.45 K are even broader ($\Gamma = 0.85 \pm 0.2$ mm/sec). Since all spectra have the central line, and since this line completely dominates at low concentrations in all matrices, we ascribe this line to the presence of isolated ^{57}Fe atoms which do not have another iron atom as one of their nearest neighbors. This isolated iron atom we call the monomer, and we assume that it has the electron configuration $3d^6 4s^2$. The two narrow lines, which intensify at higher concentrations in argon and krypton and seem to appear at 1.45 K in xenon, can be interpreted as being the result of the quadrupole splitting of the $I = \frac{3}{2}$ excited nuclear state of ^{57}Fe in the axially symmetric electric field gradient produced by an iron nearest neighbor. This we refer to as the dimer. In Sec. III H the experimentally determined dimer/monomer ratios are compared
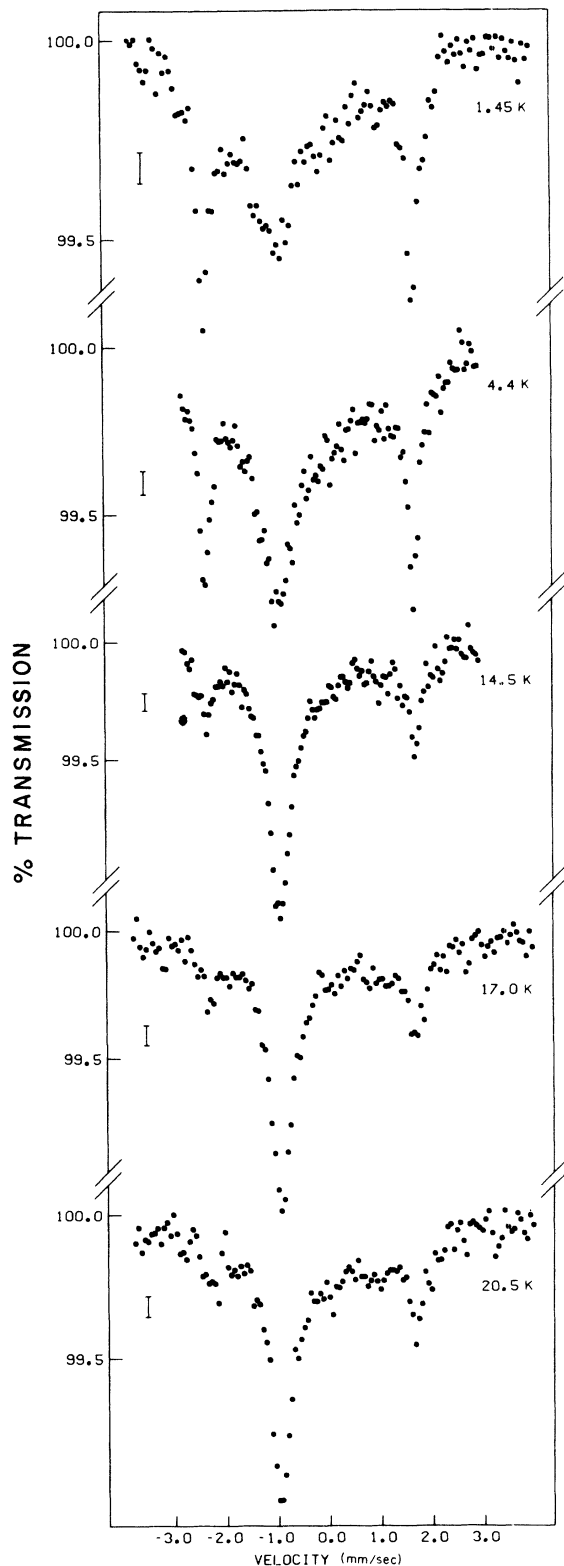
FIG. 1. Mössbauer absorption spectra of ^{57}Fe in an argon matrix. Ar/Fe = 105; 75 μg/cm^2 iron (90% enriched ^{57}Fe). Matrix temperatures between 1.45 and 20.5 K.
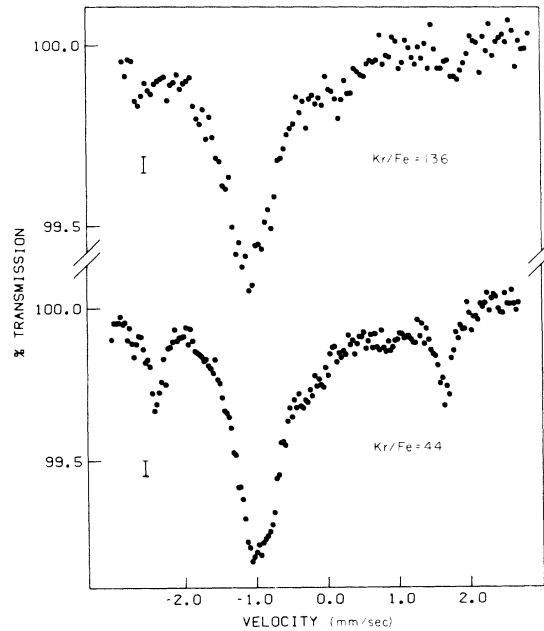

FIG. 2. Mössbauer absorption spectra of ^{57}Fe in krypton matrices at 4.4 K for different iron concentrations. Upper spectrum: Kr/Fe = 136; 37 μg/cm^2 iron (90% ^{57}Fe). Lower spectrum: Kr/Fe = 44; 65 μg/cm^2 iron (90% enriched ^{57}Fe).

with the theoretical ratios calculated from probability considerations.

B. Monomer Isomer Shift

The Mössbauer-effect isomer shift is given by Shirley[15] as

$$\delta = \left(\frac{4\pi Z e^2 R^2 c}{5E_\gamma}\right) S'(Z) \left(\psi_A^2(0) - \psi_S^2(0)\right)\frac{\delta R}{R} \ , \qquad (1)$$

where R is the nuclear charge radius and δR is the change in the charge radius between the excited and ground state of the nucleus. $\psi^2(0)$ is the nonrelativistic electron density at the nucleus, and the subscripts refer to the source (S) and the absorber (A). $S'(Z)$ is a term that corrects the electronic wave functions for relativistic effects [$S'(Z) = 1.29$ in iron[15]].

There is a difficulty in correlating isomer-shift data and electron densities at the iron nucleus. This arises from the uncertainty in the application of free-atom or -ion wave functions and in the choice of electron configurations for particular reference compounds. Despite these uncertainties, Walker et al.[16] used Watson's[17] free-ion wave functions in an analysis of ^{57}Fe isomer-shift data to derive a value for $\delta R/R = -1.8 \times 10^{-3}$. However, the relativistic correction was not used in their calculation; applying this correction changes $\delta R/R$ to -1.4×10^{-3}. This work and subsequent attempts at isomer-
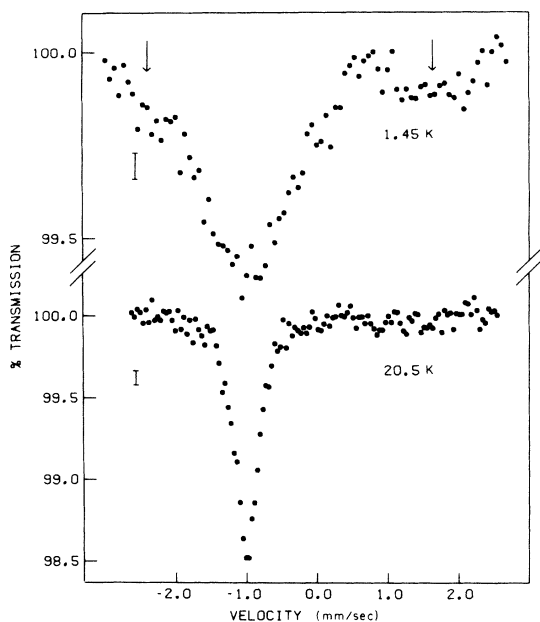
FIG. 3. Mössbauer absorption spectra of ^{57}Fe in a xenon matrix. Xe/Fe =40; 50 $\mu g/cm^2$ iron (90% enriched ^{57}Fe). Matrix temperatures 1.45 and 20.5 K.

shift data interpretation in ^{57}Fe have been reviewed by Danon[18] and Shirley.[19] An upper limit for $|\delta R/R|$ = 4.0×10^{-4} (when the relativistic correction is applied) is claimed by Simanek and Wong[20] from the pressure dependence of the isomer shift of KFeF$_3$. To date, however, most investigators have found $\delta R/R$ to lie between this value and that determined by Walker et al.[16]

Pleiter and Kolk[21] have carried out an alternative calibration of the ^{57}Fe isomer shift by combining Mössbauer-effect studies with conversion-electron spectroscopy. In this, $\psi^2_{4s}(0)$ is determined from the relative conversion rates for the 3s and 4s electrons and calculated[17] $\psi^2_{3s}(0)$ values. When combined with the isomer shifts on the same sources, $\delta R/R$ = - (4.5±1.5)×10^{-4}. In the data analysis it was assumed that the shapes of the M and N internal conversion lines are identical and that therefore the ratio of the heights gives the relative internal conversion rates. Porter and Freedman[22] have shown, however, that the N_1 and M_1 shells have markedly different conversion line shapes. They show that the spectral resolution must be sufficient to delineate the complete line shape in order that an accurate line-area determination can be made. They further show that the assumption of identical shapes of the M_1 and N_1 internal conversion lines give too high N_1/M_1 ratios, i.e., too high 4s electron densities. This effect would produce a too low $|\delta R/R|$ value in Pleiter and Kolk's analysis.

All of our isomer-shift measurements of the ^{57}Fe monomer imbedded in argon, krypton, and xenon be-

tween 1.45 and 20K are consistent with the value - 0.75±0.03 mm/sec with respect to an iron metal absorber at 300 K. (The Doppler velocities given in Figs. 1–3 are absolute velocities with respect to the ^{57}Co/Pd source at 300 K.) Second-order Doppler shifts[23] in argon, krypton, and xenon, as estimated from the Debye temperatures of the rare-gas solids,[24] are of the order of 0.01 mm/sec at 20 K and have been neglected. The result, that the isomer shift of the monomer is identical within the error for each of the three matrices, agrees well with the optical spectroscopic data, as discussed in the Introduction, which show that the matrix has only a minimal effect on the atomic configuration of the trapped atoms.

The monomer datum gives one of two required isomer shifts for the determination of $\delta R/R$. For the other isomer shift we shall use FeF$_2$, and assume, as have most investigators,[18,19] that it is representative of the atomic configuration $3d^6 4s^0$. Free-ion calculations[17] give a difference of 6.0 a.u. in $\psi^2(0)$ between the configurations $3d^6 4s^2$ and $3d^6 4s^0$. Goldanskii et al.[25] have attempted to determine the degree of covalent bonding in FeF$_2$ and find that $3d^{6.06} 4s^{0.06} 4p^{0.18}$ is a more realistic configuration.

The isomer shift of FeF$_2$ at 4.2 K is[26,27] 1.57 ± 0.01 mm/sec relative to an iron absorber at 300 K. Combining the monomer datum with that for FeF$_2$ gives $\delta R/R$ = - (10.6±0.2)×10^{-4}.

Note added in proof. Hartree-Fock calculations by Blomquist et al. [J. Blomquist, B. Roos, and M. Sundbom, J. Chem. Phys. $\underline{55}$, 141 (1971)] give a difference of 7.0 a.u. in $\psi^2(0)$ between the configurations $3d^6 4s^2$ (^5D) and $3d^6 4s^0$ (^5D). With this new value for $\Delta\psi^2(0)$ we get $\delta R/R$ = - (9.1±0.2) ×10^{-4}.

If the covalency correction of Goldanskii et al.[25] is included, then this value is increased by approximately 2.5%. The quoted error is only the experimental error. Uncertainties in Watson's calculation of $\psi^2_{4s}(0)$ were not taken into account.

Ingalls[28] has analyzed the isomer shift of ^{57}Fe in solids in terms of band structure. For an effective atomic configuration of $3d^{8-x} 4s^x$ for iron in iron metal he obtains $x = 1.5$. By comparing the isomer shift of ^{57}Fe in iron metal with the isomer shift of the monomer ($3d^6 4s^2$) and FeF$_2$ ($3d^6 4s^0$), we obtain a value of $x = 1.45 ± 0.04$.

C. Monomer Linewidth

The matrix temperature influences the monomer linewidth in the following two different ways.

(i) There is an irreversible narrowing of the monomer line when the matrix temperature is raised from 4 to 20 K and then reduced back to 4 K. This irreversible reduction in the linewidth is the largest for ^{57}Fe in an argon matrix and is not seen

TABLE I. Monomer linewidths Γ at $T = 4.4$ K before and after annealing. Annealing temperatures: Ar: 18K; Kr: 20.5 K; and Xe: 27 K. Iron concentrations: Ar/Fe = 105, Kr/Fe = 80, and Xe/Fe = 40.

	Ar	Kr	Xe
Γ (mm/sec) before	1.6 ± 0.1	0.86 ± 0.04	0.75 ± 0.03
Γ (mm/sec) after	1.0 ± 0.06	0.74 ± 0.04	0.75 ± 0.03

(ii) We observe a *reversible narrowing* of the monomer line with increasing temperature (Fig. 4). Let us define the linewidth change $\Delta\Gamma = \Gamma - \Gamma_0$, where $\Gamma_0 = 0.22$ mm/sec is the lowest linewidth observed with our apparatus. $\Delta\Gamma$ then is the same within the experimental errors for iron in a krypton and xenon matrix, and is in the the temperature region $T = 1.45-20.5$ K proportional to $1/T$. For ^{57}Fe in an argon matrix $\Delta\Gamma$ is larger than in a kryp-

for ^{57}Fe in a xenon matrix (even when the xenon-matrix temperature is increased to 27 K) (see Table I). It can be explained by annealing of the rare-gas matrices. An imperfect rare-gas lattice with non-cubic crystalline fields at the iron atom sites will broaden the line due to their interaction with the ^{57m}Fe nuclear electric quadrupole moment. An environment with fewer dislocations will therefore lead to a narrower line. The annealing temperatures for interstitials and vacancies are lowest for argon and highest for xenon; this can be seen from a comparison of the rare-gas binding energies,[24] together with the law of corresponding states.[29] Therefore, it is to be expected that an increasing of the matrix temperature to 20 K will have the largest annealing effect in argon and the smallest in xenon. In a similar way the narrowing of the monomer linewidth with increased iron concentration[14] can be explained. In order to obtain higher concentrations of iron in a rare-gas matrix, the furnace temperature is increased and the rare-gas flow reduced. The time available to trap iron and rare-gas atoms onto a cubic site at the matrix surface (surface diffusion time) is approximately the time between the deposition of adjacent "layers" of the rare gas. The lower gas flow rate at high iron concentrations allows a longer surface diffusion time and therefore leads to a less dislocated matrix. The experiments show further that even an annealed (20 K) krypton matrix with low iron concentration ($\phi = 0.0125$) has a larger linewidth ($\Gamma = 0.75 \pm 0.04$ mm/sec) than an unannealed krypton matrix with higher iron concentration ($\phi = 0.022$, $\Gamma = 0.67 \pm 0.03$ mm/sec). This means that a temperature of 20 K is not enough to anneal all these crystal imperfections which are created in a krypton matrix in a low-iron-concentration run.

It has also been observed[30] in the optical-absorption spectrum of iron atoms in a krypton matrix that narrower absorption lines are obtained when the matrices are annealed at 20.5 K or the krypton gas flow rate is reduced. This is for the same reason as in the Mössbauer studies, since ill-defined crystalline environments (not cubic symmetry) give rise to additional crystal-field splittings and hence to line broadening.
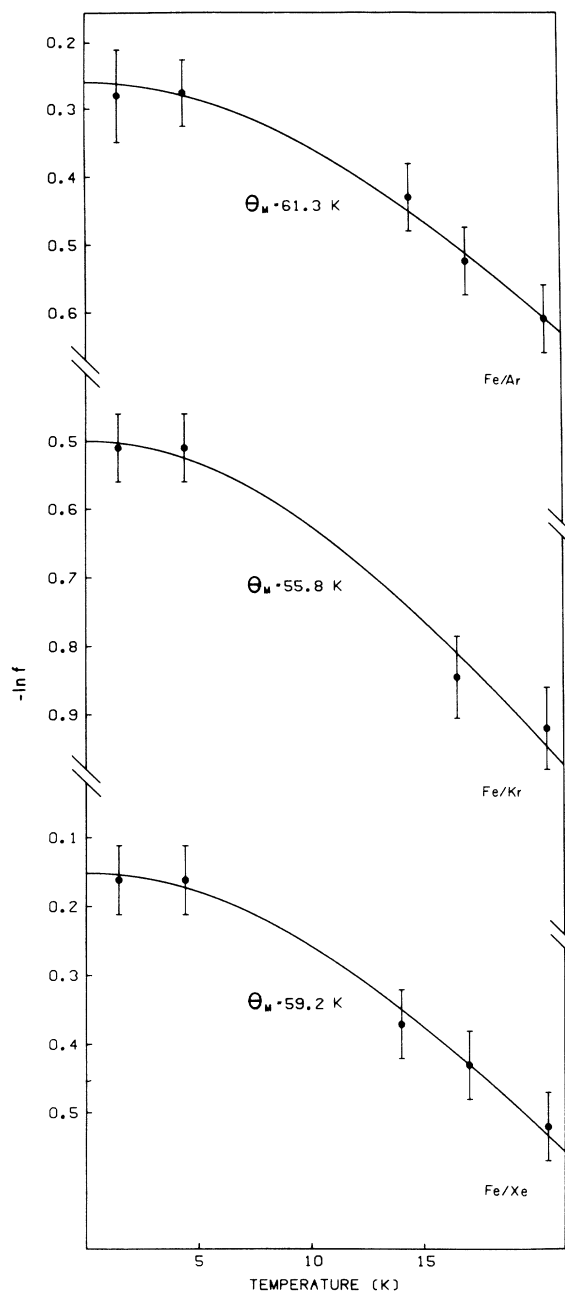

FIG. 4. Temperature dependence of monomer linewidth for ^{57}Fe in argon, krypton, and xenon matrices.

ton or xenon matrix at a given matrix temperature, and $\Delta\Gamma \propto 1/T$ breaks down for $T \lesssim 4$ K since Γ seems to approach a constant value. The optical-absorption spectra of iron in rare-gas matrices show that there is only a very small difference in the fine-structure splitting of the iron atomic levels between the free iron atom and the rare-gas–matrix-isolated iron atom [for instance $\Delta\nu(3d^7 4p\,^5D_4 - 3d^7 4p\,^5D_3) = 413$ cm^{-1} for the free iron atom, and 380 ± 10 cm^{-1} for iron in a krypton matrix[1,30]]. This means that the rare-gas matrix does not appreciably change the spin-orbit coupling in the iron atom. The orbital momentum ($L = 2$) is therefore not quenched by the rare-gas matrix and J is a good quantum number. From this it follows that the hyperfine magnetic field $H_{\rm hf}$ at the iron nucleus in a rare-gas matrix is approximately that of the free iron atom. This has been determined by an atomic-beam NMR experiment to be $H_{\rm hf} = (1.11 \pm 0.02) \times 10^6$ Oe.[31] One should therefore expect a large magnetic hf splitting of the nuclear energy levels (splitting of the two outer lines $\Delta \approx 35$ mm/sec). Even at the lowest matrix temperature (1.45 K) we see no such hyperfine structure. To explain this, we assume a spin-lattice relaxation time $T_1 \ll 1/\omega_L$ (ω_L is the nuclear Larmor frequency in $H_{\rm hf}$) even at 1.45 K. In the region $T_1 \ll 1/\omega_L$ the normal six-line hfs pattern collapses to a single line with a half-width of $\Gamma = \Gamma_0 + \Delta\Gamma$, where $\Delta\Gamma = (\omega_L/2\pi T_1^{-1})\Delta$.[32] From the measured $1/T$ dependence of $\Delta\Gamma$, it follows therefore that $T_1^{-1} \propto T$, which shows that the direct phonon process is dominant for the spin-lattice relaxation of ^{57}Fe in rare-gas matrices. The straight lines in Fig. 4 can be represented by $1/T_1 = AT$. The A values for the different rare-gas matrices are shown in Fig. 4 and are calculated for $H_{\rm hf} = 1.1 \times 10^6$ Oe.

We assume that the relaxation process occurs between the four sublevels of the split $^5D_4$ ground state in a cubic crystalline field where each of these sublevels may be approximately represented by some linear combination of the basis wave functions $|J, J_z\rangle$.[31] Since, for example, the optical-absorption spectrum of iron in a krypton matrix shows no crystal-field splitting of the $3d^6 4s^2\,^5D_4 - 3d^7 4p\,^5D_4(^5D_3)$ absorption lines [full width at half-

maximum (FWHM) ~ 30 cm^{-1}],[30] the splittings of the excited states $3d^7 4p\,^5D_4(^5D_3)$ must be <10 cm^{-1} and the splitting of the $3d^6 4s^2\,^5D_4$ ground state must be even smaller. These splittings seem therefore to be much smaller than $k\Theta_D$ [Θ_D is the Debye temperature of the rare-gas solid (see Table II)], thus allowing the direct phonon process for the spin-lattice relaxation mechanism. The experimental evidence for an unquenched orbital momentum together with the fact that the relaxation takes place between non-Kramers doublets leads one to expect a very short spin-lattice relaxation time.[33,34] The observed relaxation time of $T_1 \sim 2.5 \times 10^{-10}$ sec at 1.45 K for ^{57}Fe in rare-gas matrices is, however, still much shorter than, for instance, the shortest observed spin-lattice relaxation times in Mössbauer experiments with rare-earth salts (for instance, dysprosium ethyl sulfate: $T_1 \sim 10^{-8}$ sec at 5 K)[35] where there are also unquenched orbital momenta and relaxation between non-Kramers doublets.

The observed temperature dependence of $\Delta\Gamma$ for ^{57}Fe in an argon matrix at low temperatures ($T \lesssim 4$ K) can be explained by the well-known fact that the relaxation time T_{1d} for the direct phonon process goes to a constant value for $kT \ll \Delta E$. The limiting value of $\Delta\Gamma$ corresponds to the spontaneous emission of phonons and is given by[34] $\Delta\Gamma \propto T_{1d} \propto \tanh(\Delta E/2kT)$, where ΔE is the crystal-field splitting between the levels which are involved in the spin-lattice relaxation process. From this it would follow that ΔE of the iron $^5D_4$ ground state is larger in an argon matrix than in a krypton or xenon matrix. The broken line in Fig. 4 gives an extrapolated $\tanh(\Delta E/2kT)$ curve, with $\Delta E \sim 3$ cm^{-1}. This ΔE is not in disagreement with the estimated limit $\Delta E < 10$ cm^{-1}, from optical data, for the splitting of the iron $^5D_4$ ground-state level in krypton.

The fact that $\Gamma(T \to \infty)$ is larger than Γ_0 (~ 0.22 mm/sec) can be explained in the following way: Even after annealing of the matrices at 20.5 K (xenon matrix at 27 K) the ^{57}Fe atoms are not in a perfect cubic crystal field. Since $\Gamma(T \to \infty)$ is larger for argon than for krypton or xenon, it would follow that even for the highest annealing temperature the ^{57}Fe environment in an argon matrix is after annealing still not as well defined as in a krypton or xenon matrix (see Table I). A confirmation of this is to be seen in the optical-absorption spectrum of iron in argon matrices.[1,30] The spectrum of iron in argon is, even after annealing, more complicated than that for iron in krypton and xenon with approximately double the expected number of lines appearing. This might suggest either (i) a large crystal-field splitting due to a noncubic symmetry in the iron environment (for instance, there could be a vacancy as one of the nearest neighbors of the iron atom) or (ii) two different crystallographic sites for the iron atoms in the argon matrix. A quadrupolar

TABLE II. Comparison of Debye temperatures (at 10 K) as obtained from specific-heat measurements of rare-gas solids with Mössbauer temperatures Θ_M as probed by a ^{57}Fe atom in rare-gas matrices.

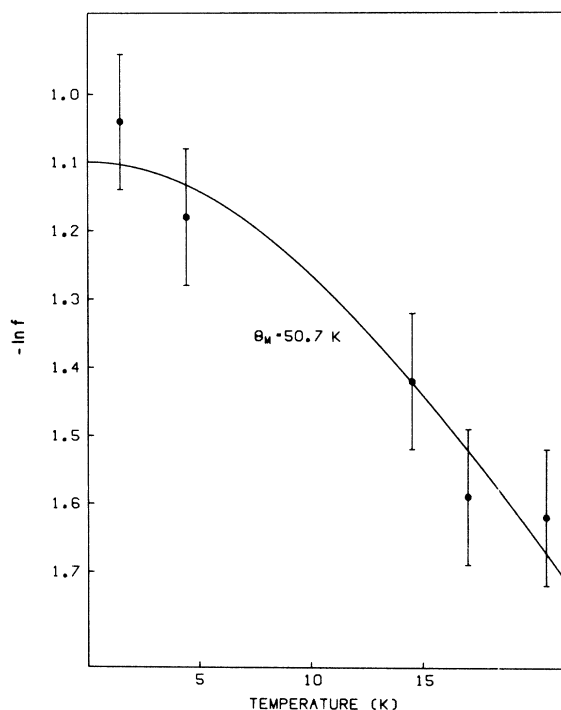|	Ar	Kr	Xe
Θ_D (K)[a]	82	63	55
Θ_D^f (K)	69	77	83
Θ_M (K)	61.3 ± 4	55.8 ± 4	59.2 ± 4

[a]See Ref. 24.

FIG. 5. Temperature dependence of Mössbauer f factor for the monomer in argon, krypton, and xenon matrices.

broadening of the Mössbauer monomer spectra would be expected in case (i) and in case (ii) only if one of the ^{57}Fe sites has noncubic symmetry.

D. Temperature Dependence of Mössbauer f Value for the Monomer

The measurement of the recoilless fraction f of absorbed γ rays at various temperatures allows the calculation of the temperature dependence of the mean-square displacement $\langle x^2(T) \rangle$ for the iron atom in the rare-gas matrices [i. e., $\ln f \propto \langle x^2(T) \rangle$]. By assuming a Debye model for the frequency spectrum with which the oscillations of the iron atom in the rare-gas matrix can be described, the characteristic Debye temperature (Mössbauer temperature Θ_M) of the rare-gas solid as probed by the Fe Mössbauer atom can be calculated[36]:

$$ -\ln f\,(T) = -\frac{3\hbar^2}{Mk\Theta_M}\left[\frac{1}{4} + \left(\frac{T}{\Theta_M}\right)^2 \int_0^{\Theta_M/T} \frac{x}{e^x - 1}\,dx\right] . $$

$$ (2) $$

Figure 5 shows the experimental results for argon, krypton, and xenon. The solid lines are best computer fits in the Debye model. The fact that a Debye model fits the experimental data very well does not necessarily imply such a simple frequency spectrum for the iron atom in a rare-gas matrix. It only

shows that $\langle x^2(T) \rangle$ of the iron atom in the rare-gas matrix can be reasonably described by such a simple model and the determined Θ_M.

In Table II the first line gives the Debye temperature Θ_D of the solid rare gases (at $T = 10$ K) determined from specific-heat measurements[24]; the second line shows the expected effective Debye temperature Θ_D^i for an impurity atom with mass M_i in a host (rare-gas) lattice with mass M_h and Θ_D^h by using the familiar approximation[37]

$$ \Theta_D^i = \Theta_D^h\,(M_h/M_i)^{1/2} . $$

$$ (2') $$

Line 3 shows the experimentally determined Mössbauer temperatures Θ_M (see Fig. 5). These are for all three matrices lower than the expected values. It should be mentioned here that the measurement of the Mössbauer effect of ^{83m}Kr in solid krypton has given a Mössbauer temperature $\Theta_M \sim 42$ K,[9,38] which is also much lower than $\Theta_D = 63$ K. Mahesh[38] explains this difference by considering the contribution of lattice anharmonicity to the recoilless fraction.

The measurement of the temperature dependence of optical-absorption lines from iron atoms in rare-gas matrices offers another possibility to determine the $\langle x^2(T) \rangle$ of such an iron atom. According to a theory of Lax,[39] the linewidth of such absorption lines should be in first approximation proportional to $(\langle x^2(T) \rangle)^{1/2}$ of the impurity atom. Such a measurement has been done with an iron-doped krypton matrix.[30] From the temperature dependence of $\langle x^2(T) \rangle$ one gets in the Debye model $(\Theta_D)_{\mathrm{opt}} = 60 \pm 5$ K. This is in good agreement with that determined by the Mössbauer effect.

E. Dimer Quadrupole Splitting

We are interpreting the pair of narrow lines appearing in the argon and krypton matrices at all temperatures, and in the xenon matrix at 1.45 K, as the quadrupole splitting of the $I = \frac{3}{2}$ excited nuclear state of ^{57}Fe in the axially symmetric electric field gradient produced by an iron nearest neighbor. The observed dimer quadrupole splitting in argon and krypton is $\Delta E_Q = 4.05 \pm 0.04$ mm/sec, independent of the rare-gas matrix and matrix temperature. The two peaks appearing in the 1.45-K xenon experiment (see arrows in Fig. 3) are too weak to allow an accurate determination of the dimer quadrupole splitting in xenon.

For a nucleus with spin $\frac{3}{2}$ and quadrupole moment Q the quadrupole splitting is[40]

$$ \Delta E_Q = \tfrac{1}{2}e^2q\,Q , $$

$$ (3) $$

where q is the electric field gradient (EFG) at the nucleus.

The orbitally degenerate ^5D iron atomic ground state splits in an axial field into three levels:

TABLE III. Overlap integrals $S(4s, 4s')$ and $S(3d, 3d')$ between the 4s and 3d electron wave functions of iron (Ref. 17) for two iron atoms sitting on nearest-neighbor substitutional crystal sites in different rare-gas matrices. The nearest-neighbor distances at $T = 4$ K are 3.76, 3.99, and 4.33 Å in Ar, Kr, and Xe, respectively (Ref. 24).

| | $S(4s, 4s')$ | $S(3d, 3d')$ | | |
		$\|3z^2 - r^2\rangle$	$\|xz\rangle, \|yz\rangle$	$\|x^2 - y^2\rangle, \|xy\rangle$
Ar	0.22	1.9×10^{-3}	5.9×10^{-4}	5.9×10^{-5}
Kr	0.19	1.1×10^{-3}	3.3×10^{-4}	3.0×10^{-5}
Xe	0.15	0.45×10^{-3}	1.2×10^{-4}	1.0×10^{-5}

$\|3z^2 - r^2\rangle$; $\|xz\rangle$, $\|yz\rangle$ (twofold degenerate); $\|x^2 - y^2\rangle$, $\|xy\rangle$ (twofold degenerate). Either $\|3z^2 - r^2\rangle$ which has the largest overlap integral with the 3d wave function of the neighboring iron atom (see Table III, column 2) or $\|x^2 - y^2\rangle$, $\|xy\rangle$ which has the smallest overlap integral (see Table III, column 4) is the lowest energy level. The weak cubic crystalline field of the rare-gas solid will lift the degeneracy of the $\|x^2 - y^2\rangle$, $\|xy\rangle$ state. Both the $\|xy\rangle$ and the $\|x^2 - y^2\rangle$ state produce an EFG at the ^{57}Fe nucleus of $+\frac{4}{7}\langle r^{-3}\rangle_{3d,\text{eff}}$, and the $\|3z^2 - r^2\rangle$ state an EFG of $-\frac{4}{7}\langle r^{-3}\rangle_{3d,\text{eff}}$.[41,42] Here $\langle r^{-3}\rangle_{3d,\text{eff}}$ includes the Sternheimer correction.[43] Since the observed ΔE_Q is temperature independent in the range $1.45 \leq T \leq 20.5$ K, the splitting of the ^5D state in the axial field of the neighboring iron atom must be much greater than kT,[42] thus showing that this splitting is much larger than the splitting in the cubic crystalline field of the rare-gas solid (see Sec. III C).

For $\langle r^{-3}\rangle_{3d,\text{eff}}$ of an iron atom in the dimer we take the free iron ion value as calculated to be $\langle r^{-3}\rangle_{3d,\text{eff}} = 3.3$ a.u.[44,45] We think that this is a reasonable value to choose, since the 3d overlap integrals $S(3d, 3d')$ in Table III are very small $[S(3d, 3d') < 2 \times 10^{-3}]$. Ingalls[46] has calculated the "bare" quadrupolar coupling constant $\Delta E_0 = \frac{2}{7} e^2 Q \langle r^{-3}\rangle_{3d,\text{eff}}$ of the Fe^{2+} ion and obtained $\Delta E_0 = 4.1 \pm 0.2$ mm/sec. The agreement of our measured ΔE_Q for the dimer with this ΔE_0 is another confirmation that $\langle r^{-3}\rangle_{3d,\text{eff}}$ of an iron atom in the dimer can be replaced by the free iron ion value.

With $\Delta E_Q = 4.05 \pm 0.04$ mm/sec we obtain from formula (3) for the quadrupole moment Q of the first excited state of ^{57}Fe $Q = \pm 0.213b$. The sign of Q has been determined[47] to be positive. The error in this value is determined by the accuracy with which $\langle r^{-3}\rangle_{3d,\text{eff}}$ is calculated for the free iron ion. The experimental contribution to the error is only about 1%.

F. Dimer Isomer Shift

The dimer isomer shift is $\delta = -0.14 \pm .02$ mm/ sec (with respect to an iron foil at 300 K) for ^{57}Fe in argon and krypton and is independent of matrix temperature and iron concentration. The two peaks appearing in the 1.45-K xenon experiment (see arrows in Fig. 3) are too weak to allow an accurate determination of the dimer isomer shift in xenon. The dimer isomer shift is less negative than the monomer isomer shift, i.e., the dimer has a smaller total s electron density at the ^{57}Fe nucleus than the monomer. If we assume an effective atomic configuration for an iron atom in the dimer of $3d^6 4s^x$, then by comparison of the monomer and dimer isomer shifts we get $x = 1.47 \pm 0.04$ if we take an atomic configuration of $3d^6 4s^0$ for the iron atom in FeF_2 (see Sec. III B).

This lower total s electron density at the ^{57}Fe nucleus in the dimer in comparison to that in the monomer could be caused (i) by a decrease of the 4s electron density at the ^{57}Fe nucleus due to the large 4s overlap integral $S(4s, 4s')$ (see Table III) and/or (ii) by a change of the 3d electron wave functions due to the small 3d overlap integral $S(3d, 3d')$ (see Table III) in such a way that the s electron shielding is increased. The dimer isomer shifts are, within the errors, the same for the dimer in argon and krypton. The overlap integrals $S(4s, 4s')$ and $S(3d, 3d')$ for two iron atoms on nearest-neighbor substitutional sites in argon and krypton differ, however, by 15% and a factor of 2, respectively. This suggests that the dimer is a bound state with a constant internuclear separation.

G. Temperature Dependence of the Mössbauer f Factor for the Dimer

Only in the argon matrix does the dimer appear with a high enough probability to allow a determination of the temperature dependence of its Mössbauer f factor. Figure 6 shows the experimental results obtained for an argon matrix with $\phi = 0.01$ (see Fig. 1). We assume that the coupling between the two iron atoms in the dimer is not much stronger than the coupling between an iron and a rare-gas atom. Therefore, we put for the mass M of the recoiling nucleus in formula (2') only the mass of a single iron atom. The solid line in Fig. 6 is a best computer fit in the Debye model with $\Theta_{M,\text{dimer}} = 50.7 \pm 5$ K. This is lower than Θ_M for the monomer in argon (see Table II). That result can be explained by the superimposition on the argon phonon spectrum of the two vibrational modes of the dimer. These two modes are a high-frequency mode (local mode) corresponding to an oscillation of the two iron atoms out of phase, and a low-frequency mode (resonance) corresponding to an in-phase oscillation of the two iron atoms. The energy of the local mode might be too high to influence $\langle x^2(T)\rangle$; the resonance mode, however, will increase $\langle x^2(T)\rangle$ and therefore lower $\Theta_{M,\text{dimer}}$.
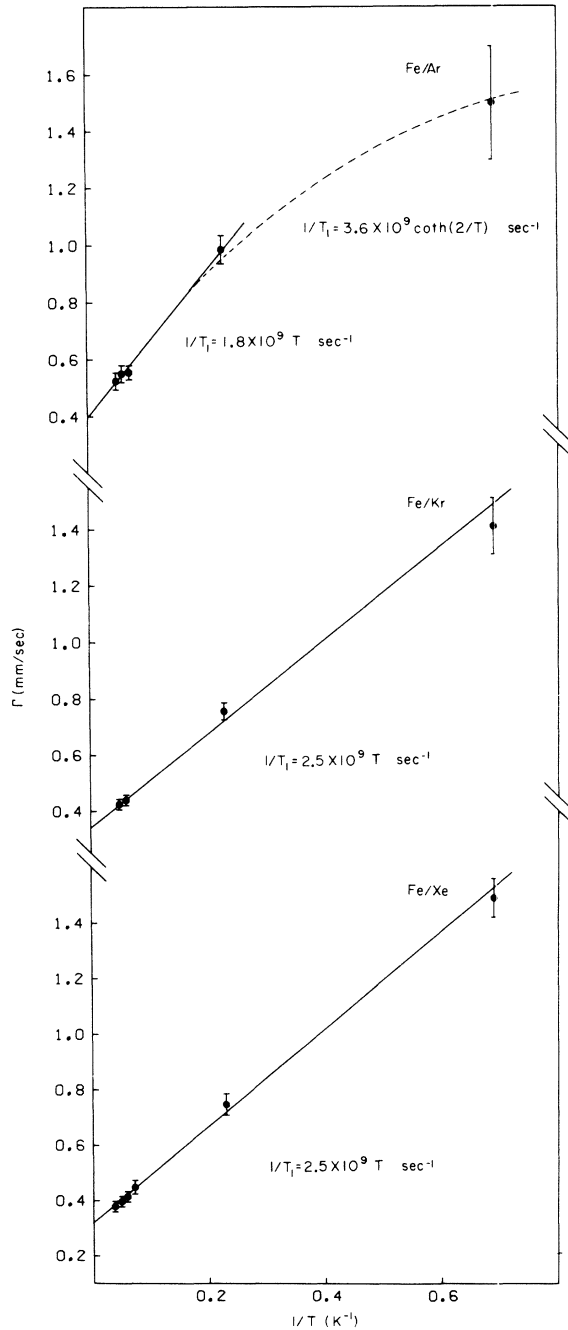
FIG. 6. Temperature dependence of Mössbauer f factor for the dimer in an argon matrix.

H. Dimer/Monomer Ratio

For the calculation of the dimer/monomer ratio from probability considerations, we assume a random distribution of the iron atoms in the rare-gas matrices. The rare-gas solids have fcc structure[24]; each lattice site has 12 nearest neighbors. The probability P_N that one iron atom has N other iron

atoms as nearest neighbors can be expressed as[48]

$$P_N = \frac{12!\,\phi N(1-\phi)^{12-N}}{(12-N)!\,N!} , \qquad (4)$$

where ϕ is the iron atomic concentration in the rare-gas matrix. The atomic concentration ϕ is related to the rare-gas/iron atomic ratio R by $\phi = 1/(R+1)$. With formula (4) the probabilities of occurrence of the monomer (P_0) and dimer (P_1) are calcuated for three different argon and krypton matrices and one xenon matrix. These values are given in Table IV, together with the calculated ratios of the dimer to monomer $[(D/M)_{calc}]$. The experimentally determined ratios $(D/M)_{expt}$ in Table IV are calculated from the ratio of the resonance absorption areas for the monomer and dimer in the Mössbauer spectra at 4.4 K for argon and krypton and at 1.45 K for Xe (that is the only ^{57}Fe/Xe spectrum which shows the dimer). In each case corrections were made to account for the different Mössbauer temperatures Θ_M of the dimer and monomer. Since $\Theta_{M,dimer}$ has been determined only for the argon matrix (see Sec. III G), this value has also been taken for the dimer in krypton and xenon.

In krypton and xenon the calculated and experimental values of (D/M) are the same within the error (see last column in Table IV), whereas in argon there appear to be approximately three times the number of dimers expected. This can be explained by a migration of the iron atoms. We assume this migration takes place during the deposition of the argon matrix (probably as a surface migration of the iron atoms), since we see no increase of the dimer relative to the monomer when the argon matrix is heated up to 20.5 K after the deposition.

IV. CONCLUSION

The isomer-shift measurement of rare-gas-matrix-isolated ^{57}Fe atoms seems to us to be an important step forward in the determination of a reliable $\delta R/R$ value for the 14.4-keV transition

TABLE IV. Calculated and experimental dimer/monomer ratios (D/M).

Matrix	ϕ	P_0	P_1	(D/M) Calc	(D/M) Expt	$\frac{(D/M)_{expt}}{(D/M)_{calc}}$
Argon	0.014	0.85	0.14	0.165	0.56	3.3 ± 0.3
	0.0095	0.895	0.105	0.118	0.40	3.4 ± 0.4
	0.0028	0.965	0.035	0.036	0.11	3.1 ± 0.5
Krypton	0.023	0.76	0.21	0.276	0.29	1.05 ± 0.2
	0.016	0.825	0.16	0.195	0.25	1.3 ± 0.3
	0.0074	0.915	0.085	0.093	0.09	0.95 ± 0.3
Xenon	0.025	0.745	0.22	0.29	0.23	0.8 ± 0.3

in the ^{57}Fe nucleus. However, it gives only one of the two necessary calibration points in the isomer-shift–versus–atomic-configuration plot; our $\delta R/R$ value is therefore only as reliable as the assumed atomic configuration of $3d^6 4s^0$ for FeF$_2$. Because of the fast spin-lattice relaxation times in the rare-gas matrices, the magnetic hyperfine pattern of an isolated ^{57}Fe atom could not be detected even at 1.45 K. The reason for such a fast spin-lattice relaxation time is not completely understood. Self-consistent field calculations for the Fe dimer would solve the problem of the dimer ground-state configuration and explain the measured dimer isomer shift as well as the missing magnetic

hyperfine interaction in the dimer. They might also confirm our assumption that the observed dimer quadrupole splitting is almost identical with the bare quadrupolar coupling constant of the Fe^{2+} ion.

ACKNOWLEDGMENTS

†Work supported by the U.S. Atomic Energy Commission.

*Present address: Argonne National Laboratory, Argonne, Ill. 60439.

‡On leave from the Department of Physics, Technische Universität, Munich, Germany.

[1] D. M. Mann and H. P. Broida, J. Chem. Phys. 55, 84 (1971), and references contained therein.

[2] M. Peyron and H. P. Broida, J. Chem. Phys. 30, 1139 (1959).

[3] L. J. Schoen and H. P. Broida, J. Chem. Phys. 32, 1184 (1960).

[4] H. Micklitz and K. Luchner, Z. Physik 227, 301 (1969).

[5] G. S. Jackel, W. H. Nelson, and W. Gordy, Phys. Rev. 176, 453 (1968).

[6] P. H. Kasai, Phys. Rev. Letters 20, 67 (1968).

[7] V. Jaccarino and G. K. Wertheim, in Proceedings of the Second International Conference on the Mössbauer Effect, Saclay, France, 1961, edited by D. M. J. Compton and A. H. Schoen (Wiley, New York, 1962), p. 260.

[8] Y. Hazony, P. Hillmann, M. Pasternak, and S. Ruby, Phys. Letters 2, 337 (1962).

[9] M. Pasternak, A. Simopoulous, S. Bukshpan, and T. Sonnino, Phys. Letters 22, 52 (1966).

[10] G. Gilbert and C. E. Violet, Phys. Letters 28A, 285 (1968).

[11] S. Bukshpan, C. Goldstein, and T. Sonnino, J. Chem. Phys. 49, 5477 (1968).

[12] P. H. Barrett and T. K. McNab, Phys. Rev. Letters 25, 1601 (1970).

[13] W. Keune and E. Lüscher, Ann. Univ. Saraviensis, Sci. 8, 92 (1970).

[14] T. K. McNab and P. H. Barrett, Mössbauer Effect Methodology (Plenum, New York, to be published), Vol. 7.

[15] D. A. Shirley, Rev. Mod. Phys. 36, 339 (1964).

[16] L. R. Walker, G. K. Wertheim, and V. Jaccarino, Phys. Rev. Letters 6, 98 (1961).

[17] R. E. Watson, MIT Solid State and Molecular Theory Group Technical Report No. 12 (unpublished); Phys. Rev. 119, 1934 (1960).

[18] J. Danon, in Chemical Applications of Mössbauer Spectroscopy, edited by V. I. Goldanskii and R. H. Herber (Academic, New York, 1968), p. 160.

[19] D. A. Shirley, Ann. Rev. Phys. Chem. 20, 25 (1969).

[20] E. Simanek and A. Y. C. Wong, Phys. Rev. 166, 348 (1968).

[21] F. Pleiter and B. Kolk, Phys. Letters 34B, 296

(1971).

[22] F. T. Porter and M. S. Freedman (unpublished).

[23] R. V. Pound and G. A. Rebka, Jr., Phys. Rev. Letters 4, 274 (1960).

[24] For data on solids of rare gases, see G. L. Pollack, Rev. Mod. Phys. 36, 748 (1964).

[25] V. I. Goldanskii, in Proceedings of the Dubna Conference on the Mössbauer Effect (Consultants Bureau, New York, 1963).

[26] G. K. Wertheim and D. N. E. Buchanan, Phys. Rev. 161, 478 (1967). The value + (1.29 ± 0.01) mm/sec at 4 K with respect to a ^{57}Co/Pd source at 300 K has been adjusted to the iron metal scale (+ 0.185 mm/sec) and corrected for different zero-point second-order Doppler shifts in FeF$_2$ and rare-gas matrices (+ 0.10 mm/sec).

[27] Y. Hazony, J. Chem. Phys 45, 2664 (1966).

[28] R. Ingalls, Phys. Rev. 155, 157 (1967).

[29] J. de Boer, Physica 14, 139 (1948).

[30] H. Micklitz and P. H. Barrett, Phys. Rev. (to be published).

[31] L. S. Goodmann and W. J. Childs, Bull. Am. Phys. Soc. 9, 12 (1964).

[32] G. K. Wertheim, Phys. Rev. 121, 63 (1961).

[33] P. L. Scott and C. D. Jeffries, Phys. Rev. 127, 32 (1962).

[34] R. Orbach, in Fluctuations, Relaxations and Resonance in Magnetic Systems, edited by D. ter Haar (Oliver and Boyd, London, 1962), p. 219.

[35] S. Hüfner, H. H. Wickman, and C. F. Wagner, in Hyperfine Structure and Nuclear Radiation, edited by E. Matthias and D. A. Shirley (North-Holland, Amsterdam, 1968), p. 952.

[36] R. L. Mössbauer and W. H. Wiedemann, Z. Physik 159, 33 (1960).

[37] W. M. Visscher, Phys. Rev. 129, 28 (1963).

[38] K. Mahesh, J. Phys. Soc. Japan 28, 818 (1970).

[39] M. Lax, J. Chem. Phys. 20, 1752 (1952).

[40] M. H. Cohen and F. Reif, in Solid State Physics, edited by F. Seitz and D. Turnbull (Academic, New York, 1957), Vol. 5.

[41] A. Abragam and F. Boutron, Compt. Rend. 252, 2404 (1961).

[42] R. Ingalls, Phys. Rev. 133, A787 (1964).

[43] R. M. Sternheimer, Phys. Rev. 80, 102 (1950); 84, 244 (1951); 95, 736 (1954); 105, 158 (1957).

[44] R. Ingalls, Phys. Rev. 128, 1155 (1962).

[45] A. J. Freeman and R. E. Watson, Phys. Rev. 131, 2566 (1963).

[46]R. Ingalls, Phys. Rev. 188, 1045 (1969).
[47]C. E. Johnson, W. Marshall, and G. J. Perlow, Phys. Rev. 126, 1503 (1962), and references contained

therein.
[48]G. W. Robinson, J. Mol. Spectry. 6, 58 (1961).

Effect of Exchange with Local Moments and Hyperfine Interaction on the Electron-Spin-Resonance Line Shape in Metals*

J. H. Pifer and R. T. Longo[†]

Physics Department, Rutgers University, New Brunswick, New Jersey 08903

(Received 10 February 1971; revised manuscript received 25 June 1971)

The electron-spin-resonance and transmission-resonance line shapes in a metal containing impurities with local moments are evaluated for arbitrary exchange, hyperfine interaction, and nuclear spin using the Bloch-like equations derived by Langreth, Cowan, and Wilkins. Classical skin-depth conditions are assumed and the drift current produced by the gradient in the magnetic field is included in the diffusion term. Computer evaluation and a physical interpretation of the results are given. The theory is compared with the experimental transmission-resonance data in Cu : Mn. It is shown that the anomalies in the data are due to hyperfine interaction and a breakdown of strong coupling at low temperatures.

I. INTRODUCTION

When Owen, Browne, Knight, and Kittel[1] first examined the electron-spin-resonance (ESR) of a magnetic impurity in a metal (Mn in Cu) they expected to observe a large g shift and line broadening of the impurity resonance due to exchange interaction with the conduction electrons. Instead, they found a narrow line near $g = 2$. Hasegawa[2] explained the data in terms of a two-part system composed of the magnetic impurity magnetization $\vec{M}_d$ and the conduction-electron magnetization $\vec{M}_s$ which relaxes to the lattice with spin-lattice relaxation time T_{sl} and cross relaxes to $\vec{M}_d$ with a time T_{sd}. By detailed balance T_{ds}, the d to s cross relaxation time is related to T_{sd} by the relation $T_{ds} = \chi_r^0 T_{sd}$, where χ_r^0 is the ratio of the impurity susceptibility χ_d^0 to the conduction-electron susceptibility χ_s^0. Hasegawa pointed out that when $\vec{M}_d$ relaxes to $\vec{M}_s$ the energy does not necessarily flow to the lattice but may be returned to $\vec{M}_d$ via T_{sd}. This double cross relaxation has the same effect as no relaxation at all. Thus, $T_{1\,\text{eff}}$, the effective relaxation time of $\vec{M}_d$, depends on the size of T_{sl} relative to T_{sd}. Hasegawa showed that

$$T_{1\text{eff}} = T_{ds}(T_{sd} + T_{sl})/T_{sd} .$$

When $T_{sl} \ll T_{sd}$, $T_{1\,\text{eff}} = T_{ds} = \chi_r^0 T_{sd}$; but when $T_{sl} \gg T_{sd}$, $T_{1\text{eff}} = T_{sl}\chi_r^0$. In this latter case, where $T_{1\text{eff}}$ is controlled by T_{sl}, the relaxation is commonly said to be bottlenecked.[3] Hasegawa also explained the lack of g shift by pointing out that when $\vec{M}_s$ and $\vec{M}_d$ have fully cross relaxed (i. e., $\vec{M}_d$ is bottlenecked) they will be parallel and unable to exert a torque

on each other.

Schultz and co-workers[4,5] have used Hasegawa's model to explain the transmission-electron-spin-resonance (TESR) data for various transition impurities in copper and silver. They assumed bottleneck conditions and explained that the observed temperature-dependent g shift was due to the inequality of g_s, the conduction-electron g value, and g_d, the impurity g value. In TESR, dilute alloys are used so that at high temperature $\chi_s^0 \gg \chi_d^0$ and the g value is near g_s. At low temperature, where $\chi_d^0 \gg \chi_s^0$, the magnetic impurity dominates the resonance signal and the g value moves down to g_d. In order to explain the linewidth data it was necessary to add an impurity spin-lattice relaxation time T_{dl}, which was comparable in size to T_{sl}.

From the TESR viewpoint, the term bottleneck is a rather unfortunate choice of terminology since it is more logical to consider the conduction electrons on the same basis as the magnetic impurities rather than as a reservoir through which $\vec{M}_d$ relaxes. In addition, one normally expects that when a bottleneck is broken the relaxation will be faster, but as the term is now used, $T_{1\text{eff}}$ becomes much slower (if T_{sl} is kept constant) as the bottleneck is broken.

Hasegawa described the exchange-coupled system with two Bloch-like equations coupled to each other by the cross relaxation and by molecular or exchange fields. These phenomenological equations have been put on a better footing by Langreth, Cowan, and Wilkins[6] (LCW) who showed from first principles that coupled Bloch-like equations properly describe the system in the limit $\gamma \hbar H_0 \ll kT$, where